Kinetic Study of the Reactions of Gas-Phase V($a^4F_{3/2}$), Cr(a^7S_3), Co($a^4F_{9/2}$), Ni(a^3F_4, a^3D_3) and Zn($4s^2\ ^1S_0$) Atoms with Nitrous Oxide

Mark L. Campbell,*,† Erica J. Kölsch, and Kelli L. Hooper

Chemistry Department, United States Naval Academy, Annapolis, Maryland 21402

Received: July 27, 2000; In Final Form: September 22, 2000

The reactivity of gas-phase V($a^4F_{3/2}$), Cr(a^7S_3), Co($a^4F_{9/2}$), Ni(a^3F_4, a^3D_3), and Zn($4s^2\ ^1S_0$) with N_2O as a function of temperature and pressure is reported. The transition metal atoms were produced by the photodissociation of an appropriate precursor molecule and detected by laser-induced fluorescence. The vanadium, chromium, and cobalt rate constants are independent of total pressure indicating bimolecular abstraction reactions. The bimolecular rate constants (in molecule^{-1} cm^3 s^{-1}) are described in Arrhenius form by $k[V(a^4F_{3/2})] = (4.7 \pm 0.7) \times 10^{-11} \exp(-10.8 \pm 0.5\ \text{kJ·mol}^{-1}/RT)$, Cr($a^7S_3$), $(5.0 \pm 1.0) \times 10^{-11} \exp(-21.1 \pm 0.7\ \text{kJ·mol}^{-1}/RT)$, and Co($a^4F_{9/2}$), $(1.9 \pm 0.3) \times 10^{-10} \exp(-48.8 \pm 0.8\ \text{kJ·mol}^{-1}/RT)$ where the uncertainties represent $\pm 2\sigma$. The reactions of nickel with N_2O are pressure dependent indicating adduct formation; however, the reaction also has a bimolecular component. The room-temperature-limiting low-pressure third-order and limiting high-pressure second-order rate constants are $(8.2 \pm 2.4) \times 10^{-32}$ molecule^{-2} cm^6 s^{-1} and $(1.3 \pm 1.2) \times 10^{-12}$ molecule^{-1} cm^3 s^{-1} in N_2 buffer, respectively. The second-order rate constant for the abstraction channel for the reaction of nickel with N_2O at 298 K is $(9.3 \pm 1.3) \times 10^{-14}$ molecule^{-1} cm^3 s^{-1}. The reaction of zinc with N_2O is very slow; at 623 K an upper limit of 1×10^{-16} molecule^{-1} cm^3 s^{-1} is set for this reaction. An assessment of the semiempirical configuration interaction model used by Fontijn and co-workers to estimate barrier heights in these reactions is made.

Introduction

The reactions of gas-phase metal atoms with nitrous oxide have recently received considerable attention due to a number of both fundamental and practical reasons.[1,2] The reactions of transition metal atoms, TM, with N_2O:

$$\text{TM(g)} + \text{N}_2\text{O(g)} \rightarrow \text{TMO(g)} + \text{N}_2\text{(g)} \qquad (1)$$

are all exothermic[3,4] due to the formation of the stable N_2 and metal oxide molecules. Despite this exothermicity, metal atom reactions with N_2O have been observed to have significant energy barriers. These barriers have been attributed to the requirement of a nonadiabatic transition along the reaction pathway.[5]

Transition metal chemistry is an intriguing field of study due to the high multiplicities of the atomic ground states and the large number of low-lying metastable states. For many TM atoms, states resulting from s^2d^{n-2} and s^1d^{n-1} configurations (where n refers to the number of valence electrons) are nearly degenerate so the electronic structure of the atom plays an important role in its reaction dynamics. The kinetics of the 3d transition metals reacting with N_2O have previously received considerable attention.[6−19] Here we report temperature-dependent studies for the remainder of the 3d transition metals reacting with N_2O. We also report results for Cr and Zn and contrast our results with previously reported results. Finally, we will compare the experimentally determined barriers for these reactions with a semiempirical method developed by Fontijn and co-workers.[20] Much more experimental data has been accumulated since Fontijn and co-workers first published their model. Thus, an evaluation of the model is justified at this time.

Experimental Section

Kinetic experiments in our laboratory utilize pseudo-first-order conditions ([TM] ≪ [N_2O]) in an apparatus with slowly flowing gas. The experimental apparatus and technique have been described in detail elsewhere.[21] A schematic of the experimental arrangement can be found in ref 21. Briefly, the reaction chamber is a stainless steel reducing four-way cross with attached sidearms and a sapphire window for optical viewing. The reaction chamber is enclosed within a convection oven (Blue M, model 206F, $T_{max} = 623$ K) with holes drilled to allow for the exiting sidearms and the telescoping of the LIF signal to the PMT.

Transition metal atoms are produced by the 248 nm photodissociation of the appropriate precursor with the output of an excimer laser (Lambda Physics Lextra 200). Some precursors require the focusing of the beam to observe the atomic signal. When focusing is required, a lense ($f = 564$ mm) is placed approximately one focal length from the reaction zone. The preferred arrangement is without a focusing lense because focusing tends to produce a greater percentage of excited-state atoms. Transition metal atoms are detected via LIF using an excimer-pumped dye laser (Lambda Physics Lextra 50/Scan-Mate 2E). The fluorescence is detected at 90° to the counter-propagated laser beams with a three-lens telescope imaged through an iris. Interference filters are used to isolate the LIF. A photomultiplier tube (Hamamatsu R375) is used in collecting the LIF which is subsequently sent to a gated boxcar sampling module (Stanford Research Systems SR250), and the digitized output is stored and analyzed by a computer. Real-time viewing

* Author to whom correspondence should be addressed.
† Henry Dreyfus Teacher-Scholar.

10.1021/jp002702g CCC: $19.00
Published on Web 10/25/2000

of the photolysis prompt emission and LIF signal are accomplished using a LeCroy Model 9360 digital oscilloscope.

The transition metal precursor is entrained in a flow of buffer gas. The diluted precursor, buffer gas, and N_2O flow through calibrated mass flow meters and flow controllers (MKS Types 1459C and 0258C, and Matheson models 8102 and 8202-1423) prior to admission to the reaction chamber. Each sidearm window is purged with a slow flow of buffer gas to prevent deposition of metal atoms and other photoproducts. Pressures are measured with MKS Baratron manometers, and chamber temperatures are measured with a thermocouple.

The delay time between the photolysis pulse and the dye-laser pulse is varied by a digital delay generator (Stanford Research Systems DG535) controlled by a computer interfaced through a Stanford Research Systems SR245 computer interface. The trigger source for these experiments is scattered pump laser light incident upon a fast photodiode. LIF decay traces typically consist of 200 data points, each point averaged from 3 to 5 laser shots.

Materials. Cyclopentadienylvanadium tetracarbonyl (Strem, 97%), bis(cyclopentadienyl)vanadium (Strem, 95%), vanadium carbonyl (Strem, purity unstated), chromium carbonyl (Aldrich, 99%), cyclopentadienylcobalt dicarbonyl (Strem, 95%), bis-(cyclopentadienyl)nickel (Strem, 99%), bis(2,2,6,6-tetramethyl-3,5-heptanedionato) zinc (Strem, 99%), N_2O (MG Industries, electronic grade, 99.999%), and N_2 (Potomac Airgas, Inc., 99.998%) were used as received.

Data Analysis and Results

Under pseudo-first-order conditions in which no production processes occur after the initial photolysis event, the decrease in the [TM] with time following the photolysis laser pulse is given by

$$-\mathrm{d[TM]}/\mathrm{d}t = (k_{obs}[N_2O] + k_0)[TM] = (1/\tau)[TM] \quad (2)$$

where k_{obs} is the observed second-order rate constant due to N_2O at fixed buffer gas pressure, k_0 represents the depletion rate constant due to the reaction of transition metal with precursor molecules and fragments and diffusion out of the detection zone, and τ is the observed time constant for transition metal depletion in the presence of a given $[N_2O]$, precursor, and buffer gas pressure. The LIF signal at time t after photolysis is proportional to [TM]. Thus,

$$\mathrm{LIF} = \mathrm{LIF}_o \exp(-t/\tau) \quad (3)$$

where LIF_o is the initial LIF signal immediately following the photolysis laser pulse. LIF decays which exhibit single-exponential behavior are fitted using a least-squares procedure to determine τ. Typical plots of exponential decay are shown for vanadium and nickel in Figure 1.

As a result of the photolysis of the transition metal precursor, atoms in excited states are often produced in significant quantities. These excited state atoms possibly complicate the temporal profile of the ground state. For a ground state in which quenching of excited states after the initial photolysis laser pulse is important, the time dependence of the ground state's concentration will exhibit biexponential behavior. If this situation is not handled properly, significant errors in the determination of the values of the rate constants can occur. For cases where the decay rate of an excited state down to the ground state is fast compared to the removal rate of the ground state, cascade processes are unimportant at long times and the ground-state removal rate is determined by analysis of the decay at long

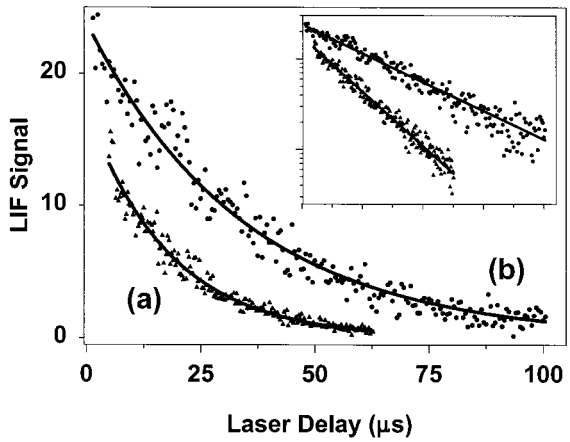

Figure 1. Typical decay curves with added N_2O in N_2 buffer at 296 K; (a) V($a^4F_{9/2}$), $T = 373$ K, $P_{total} = 20.0$ Torr, $P(N_2O) = 1.38$ Torr, $\tau = 18$ μs; (b) Ni(a^3D_3): $T = 298$ K, $P_{total} = 50.0$ Torr, $P(N_2O) = 4.14$ Torr, $\tau = 33$ μs. The solid lines through the data are least-squares fits. The inset is a ln plot of the data.

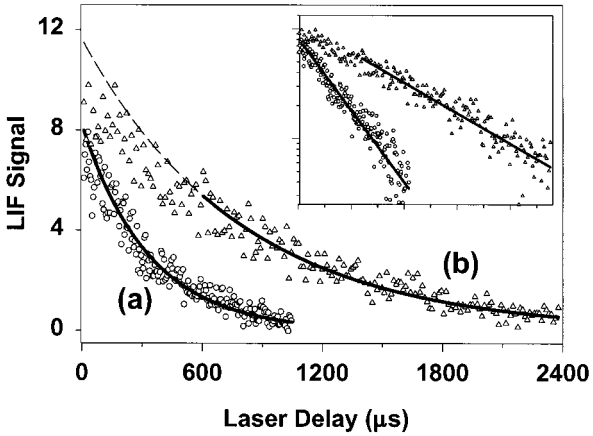

Figure 2. Typical Co($a^4F_{9/2}$) decay curves with added N_2O in nitrogen buffer at 523 K and $P_{total} = 75$ Torr; (a) $P(N_2O) = 54$ Torr, $\tau = 330$ μs; (b) $P(N_2O) = 16$ Torr, $\tau = 780$ μs. The solid lines through the data are least-squares fits. The inset is a ln plot of the data.

times. Biexponential behavior of this type has been observed for numerous transition metals.[17,22−26] Figure 2 illustrates this type of behavior which was observed for cobalt. When analyzing data with a biexponential component, it is critical that the time constant does not include contributions from the growth due to decay of short-lived excited states. Care must be taken to analyze only the section of the decay that represents the decay of the ground state. In Figure 2, the solid line indicates the range of data used to calculate the value of the time constant.

Using our experimental method, atomic lifetimes between 10 and 10000 μs can be reliably measured. Time constant measurements of less than 10 μs can be measured; however, these short values are generally not as reliable as the longer time constants. For very short values of τ, interference from cascading of excited states to the observed state is more likely to affect the decay profile. Furthermore, in some cases, overlap of the prompt emission from the photolysis event with the LIF signal at short times causes interference. Therefore, we generally attempt to perform experiments under conditions which set a lower limit for τ of approximately 10 μs.

Once the reaction time constant has been determined for a series of nitrous oxide concentrations, the slope of a plot of $1/\tau$ vs $[N_2O]$ yields the observed second-order rate constant, k_{obs}. Figures 3−5 illustrate examples of these types of plots for vanadium, cobalt, and nickel, respectively. When an atom is

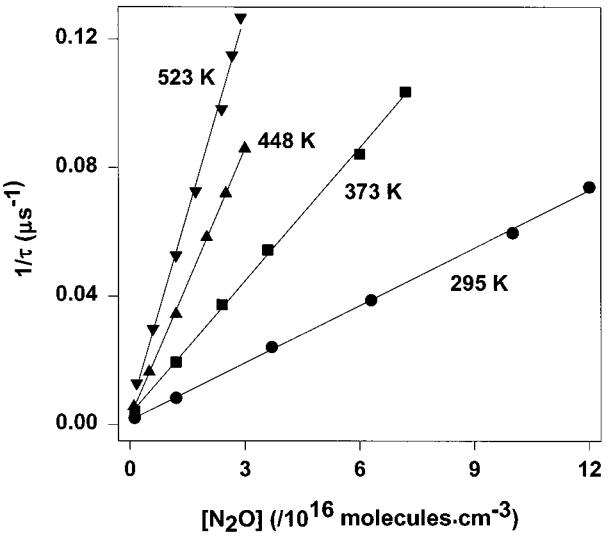

Figure 3. Typical plots for determining k_{2nd} for $V(a^4F_{3/2}) + N_2O$. The solid line for each set of data is a linear regression fit from which k_{2nd} is obtained.

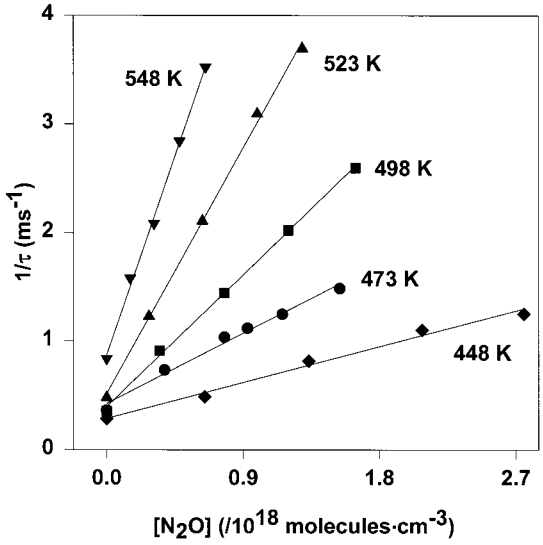

Figure 4. Typical plots for determining k_{2nd} for $Co(a^4F_{9/2}) + N_2O$. The solid line for each set of data is a linear regression fit from which k_{2nd} is obtained.

not very reactive, only a small change in the reaction time constant is observed with the addition of the oxidant. Large errors can be introduced into the value of the rate constant if the range of the time constants used to determine the rate constant is small. Thus, for unreactive atoms, high partial pressures of the oxidant are required to observe substantial changes in the time constant. For our experiments, we attempt to measure rate constants under conditions in which the time constant changes by at least a factor of 10. For some transition metals which are quite unreactive, this goal is not attainable. However, we will not report rate constants unless we observe a change in the time constant of at least a factor of 3 because the reliability of these values is low. The relative uncertainty (i.e., the reproducibility) of the second-order rate constants is estimated at ±20% based on repeated measurements of rate constants under identical temperature and total pressure conditions. The absolute uncertainties are conservatively estimated to be ±30% and are based on the sum of the statistical scatter in the data, uncertainty in the flowmeter and flow controller readings (5%) and the total pressure reading (1%), uncertainties due to incomplete gas mixing, and uncertainties due to

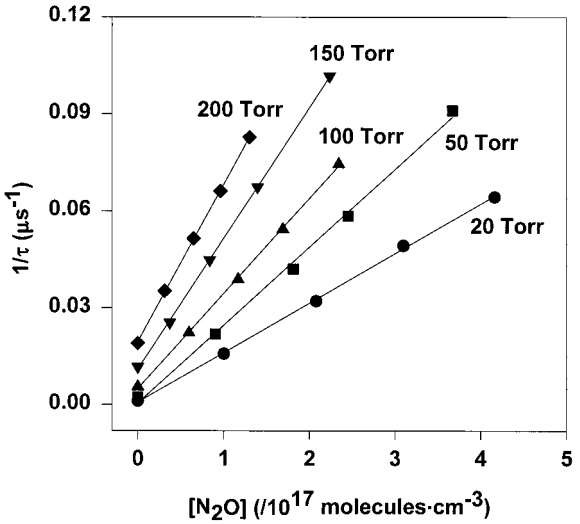

Figure 5. Typical plots for determining k_{2nd} for $Ni(a^3F_4, a^3D_3) + N_2O$ at 298 K illustrating the dependence of the bimolecular rate constants on total pressure. The solid line for each set of data is a linear regression fit from which k_{2nd} is obtained.

incomplete relaxation of the excited electronic states to the ground state.

Many of the reactions of transition metal atoms with nitrous oxide are very slow. In some cases, the rates are slower than the detection limit of the experimental method. For our experimental arrangement, the detection limit for the measurement of rate constants depends on the transition metal being studied. This variation in the detection limit as a function of transition metal atom is due to a couple of factors: (1) the conditions necessary to attain a measurable LIF signal, and (2) the lifetime of the transition metal in the absence of oxidant.

In many cases, the conditions required to attain a measurable LIF signal limit the pressure at which an experiment can be performed. We have observed that for many transition metal atoms, the LIF signal decreases as the total pressure in the reaction chamber increases. Oftentimes the LIF signal completely vanishes at high pressures. The most likely reason for the decreased signal at higher pressures is due to the physical and/or chemical quenching of the upper state of the LIF transition.

If an atom can be observed under relatively high pressure conditions, it will have a smaller detection limit than an atom which can only be observed at relatively low pressures. If an atom reacts very slowly, then a high partial pressure of the reactant will be required to make a measurable change in the lifetime of the atom. Thus, an atom which can be observed at 200 Torr will have a detection limit for its rate constants approximately a factor of 10 smaller than an atom which is limited to experiments at 20 Torr.

The second factor which determines the detection limit is the lifetime of the transition metal in the absence of oxidant. For transition metals with very long lifetimes, the detection limit will be small. A transition metal with a short lifetime in the absence of oxidant will have a proportionally higher detection limit. For the transition metals reported here, cobalt and zinc exhibited slow enough reactions at some temperatures such that the rate constants are smaller than the detection limit of our system; therefore, for these atoms only upper limits for the rate constants could be determined at these temperatures.

$V(a^4F_{3/2})$. Temperature-dependent rate constants were measured from 296 to 523 K utilizing $V(CO)_6$, $V(C_5H_5)(CO)_4$, and $V(C_5H_5)_2$ as precursors. The rate constants were independent

TABLE 1: Second-Order Rate Constants[a] ($/10^{-13}$ molecule^{-1} cm^3 s^{-1}) for the Transition Metal Reacting with N_2O

temp (K)	V($a^4F_{3/2}$)	Cr(a^7S_3)	Co($a^4F_{9/2}$)	Ni(a^3F_4, a^3D_3)[b]
298[c]	5.5	0.11		0.9
323	8.3			
333	9.0	0.30		
348	11.	0.36		1.4
373	15.	0.60		1.6
398	18.	0.85		2.0
423	22.	1.2		2.2
448	28.	1.7	0.0037	2.6
473	29.	2.3	0.0076	3.1
498	33.	3.1	0.014	3.1
523	40.	4.1	0.025	4.2
548	41.		0.041	4.7
573	50.			5.9
598				6.6
623				6.9

[a] Absolute uncertainties are estimated at ±30%. [b] Rate constants measured at 2.5 Torr. [c] Room temperature varied from 295 to 299 K.

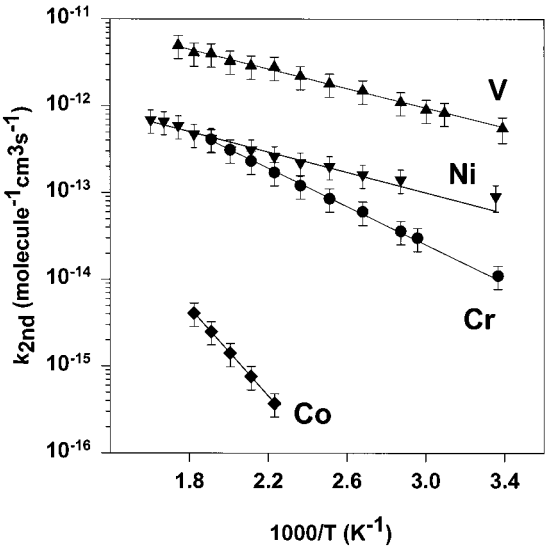

Figure 6. Arrhenius plots for the TM reactions with N_2O. Error bars represent ±30% uncertainty. The solid lines are fits to the equation $k(T) = Ae^{-Ea/RT}$.

of the precursor used. Rate constants above 523 K could not be determined due to the decomposition of the precursors. Detection of vanadium atoms was accomplished by exciting the $y^6F_{1/2}°-a^4F_{3/2}$ transition at 403.278 nm and detecting the $y^6F_{1/2}°-a^6D_{3/2}$ transition at 441.647 nm by isolating the fluorescence using a 450 nm broadband interference filter. The room-temperature rate constants were measured at 10, 20, and 50 Torr; the rate constants are independent of total pressure, confirming a bimolecular abstraction mechanism. The bimolecular rate constants are listed in Table 1. The rate constants are described in Arrhenius form by $k(T) = (4.7 \pm 0.7) \times 10^{-11}$ exp(-10.8 ± 0.5 kJ/mol/RT) molecule^{-1} cm^3 s^{-1} where the uncertainties represent $\pm 2\sigma$. An Arrhenius plot of the rate constants is shown in Figure 6.

The first reported rate constants for this reaction were room-temperature measurements determined using a fast-flow tube by Weisshaar and co-workers.[8] The reported rate constants at 300 K in helium buffer are $(4.5 \pm 0.2) \times 10^{-13}$ and $(4.8 \pm 0.5) \times 10^{-13}$ molecule^{-1} cm^3 s^{-1} at 0.8 and 0.4 Torr, respectively. These values are slightly lower than the room-temperature rate constant reported here, although the latter value is within the experimental error of our rate constant.

Cr(a^7S_3). Temperature-dependent rate constants from 296 to 523 K in argon buffer gas have been performed using $Cr(CO)_6$ as precursor. Rate constant measurements above 523 K could not be determined due to decomposition of the precursor. Detection of chromium atoms was accomplished by exciting the $z^5P_2°-a^7S_3$ transition at 373.081 nm and detecting the $z^5P_2°-a^5S_2$ transition at 520.604 nm by isolating the fluorescence using a 520 nm narrowband interference filter. The bimolecular rate constants are listed in Table 1. The rate constants are described in Arrhenius form by $k(T) = (5.0 \pm 1.0) \times 10^{-11}$ exp(-21.1 ± 0.7 kJ/mol/RT) molecule^{-1} cm^3 s^{-1}. An Arrhenius plot of the rate constants is shown in Figure 6.

Two groups have reported rate constants for the reaction of chromium with N_2O. The first reported rate constants were from Mitchell and co-workers using laser multiphotodissociation of $Cr(CO)_6$ at 559 nm in a static pressure cell.[9] The chromium atoms were probed using LIF. Second-order rate constants at two temperatures were reported, $(1.0 \pm 0.1) \times 10^{-14}$ and $(3.3 \pm 0.1) \times 10^{-14}$ molecule^{-1} cm^3 s^{-1} at 298 and 348 K, respectively. The rate constants at 298 K were found to be independent of total pressure from 0 to 150 Torr indicating bimolecuar abstraction. The Arrhenius activation energy was estimated at 21 kJ/mol based on these measurements.

Fontijn and co-workers performed an extensive study of this reaction from 278 to 1150 K using the LP/LIF method.[13] Rate constants were measured over the pressure range 45−79 mbar. Rate constants were found to be independent of total pressure. $Cr(CO)_6$ was used as the precursor at low temperatures, and $CrCl_3$ or $CrCl_3 \cdot 6H_2O$ were used at higher temperatures. The Arrhenius fit to their rate constants reported in ref 13 is incorrect; i.e., their stated equation does not fit their data. A correct weighted fit to the data yields $k(T) = (6.4 \pm 2.6) \times 10^{-11}$ exp(-20.5 ± 3.1 kJ/mol/RT) which is consistent within experimental uncertainty to the data reported here.

Co($a^4F_{9/2}$). Temperature-dependent rate constants were measured from 448 to 548 K in N_2 buffer utilizing $Co(C_5H_5)(CO)_2$ as precursor. Rate constants below 448 K could not be reliably determined due to the slow rate of the reaction, while rate constants at temperatures above 548 K could not be determined due to decomposition of the precursor. Detection of cobalt atoms was accomplished by both exciting and detecting the fluorescence from the $z^4D_{7/2}°-a^4F_{9/2}$ transition at 341.263 nm. The rate constant at 473 K was measured at 100 and 200 Torr; these rate constants are independent of pressure, indicating a bimolecular abstraction mechanism. The bimolecular rate constants are listed in Table 1. The rate constants are described in Arrhenius form by $k(T) = (1.9 \pm 0.3) \times 10^{-10}$ exp(-48.8 ± 0.8 kJ/mol/RT) molecule^{-1} cm^3 s^{-1}. An Arrhenius plot of the rate constants is shown in Figure 6.

Honma and co-workers reported an upper bound of 5×10^{-14} molecule^{-1} cm^3 s^{-1} for the room-temperature rate constant for this reaction using a fast-flow tube.[18] This upper bound is consistent with the extrapolated value determined from the Arrhenius parameters reported here.

Ni(a^3F_4, a^3D_3). Nickel has two low-lying states. The ground state is the s^2d^8 a^3F_4 state, and the low-lying s^1d^9 a^3D_3 metastable state is only 204 cm^{-1} above the ground state. The rate constants for nickel were determined primarily by monitoring the a^3D_3 state because the LIF signal of this state was much stronger than the signal for the a^3F_4 state. Several rate constants were determined for both states under identical conditions and found to be equal to within experimental uncertainty; thus, apparently an equilibrium is rapidly established between these two states

TABLE 2: Room-Temperature[a] Second-Order Rate Constants[b] ($/10^{-13}$ molecule^{-1} cm^3 s^{-1}) for Nickel Reacting with N_2O

pressure (Torr)	k
2.5	0.9
5.0	1.0
10.	1.2
15.	1.4
20.	1.6
50.	2.3
75.	2.6
100.	2.9
125.	3.5
150.	4.0
200.	4.9

[a] Room-temperature varied from 295 to 299 K. [b] Absolute uncertainties are estimated at ±30%.

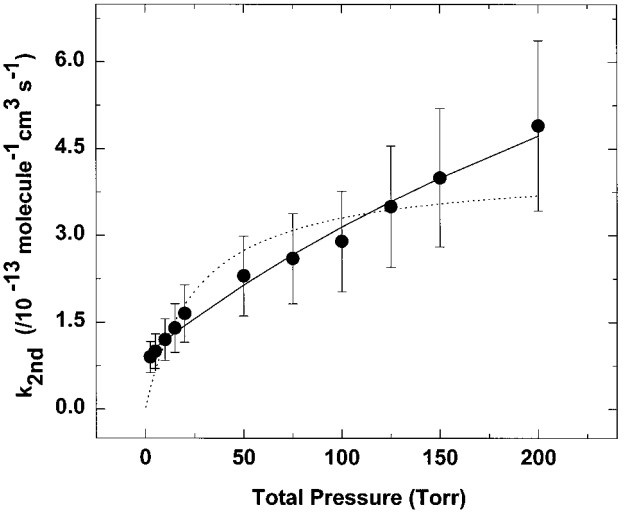

Figure 7. Pressure dependence of the reaction of Ni(a^3F_4, a^3D_3) with N_2O in N_2 buffer at 298 K. Error bars represent ±30% uncertainty. The solid line is a fit to eq 4. The dotted line is the fit to the Lindemann−Hinshelwood equation.

so that both states behave similarly with respect to chemical removal by N_2O.

Temperature-dependent rate constants were measured from 296 to 623 K using $Ni(C_5H_5)_2$ as precursor. Detection of nickel atoms was accomplished by both exciting and detecting the fluorescence from the $z^3F_4°-a^3F_4$ transition at 339.105 nm and the $z^3F_4°-a^3D_3$ transition at 341.476 nm. The room-temperature rate constants were measured over the pressure range 2.5−200 Torr (Table 2). The pressure dependence of the rate constants indicates the termolecular channel is important. However, a fit of the rate constants to the simplified Lindemann−Hinshelwood equation[27] gave unsatisfactory results. Furthermore, the rate constants (Table 1) increase with increasing temperature. The combination of these two circumstances implies a bimolecular abstraction channel is also indicated along with the adduct-formation channel. The variation with total pressure of the second-order rate constants at room temperature in nitrogen buffer gas are shown in Figure 7. The dashed line in Figure 7 is the fit to the Lindemann−Hinshelwood equation. A better fit to the data is obtained by fitting the rate constants to the equation:

$$k_{obs} = \frac{k_o[N_2]}{1 + k_o[N_2]/k_\infty} + k_{abs} \qquad (4)$$

where k_o is the limiting low-pressure third-order rate constant, k_∞ is the limiting high-pressure second-order rate constant, and k_{abs} is the rate constant for the bimolecular abstraction channel. The solid line through the data in Figure 7 is a weighted fit to eq 4. The values for k_o, k_∞, and k_{abs} for the reaction of N_2O in nitrogen buffer at 298 K are (8.2 ± 2.4) × 10^{-32} molecule^{-2} cm^6 s^{-1}, (1.3 ± 1.2) × 10^{-12} molecule^{-1} cm^3 s^{-1}, and (9.3 ± 1.3) × 10^{-14} molecule^{-1} cm^3 s^{-1}, respectively.

In fitting the rate constants to eq 4, the assumption is made that the abstraction channel is independent of the termolecular channel; however, this may not be the case. There is the possibility that the mechanism for this reaction resembles the mechanism proposed for the reaction of Al + CO_2; i.e., an energized intermediate is formed which can decompose along three different paths.[28,29] If the mechanism for the reaction of nickel with N_2O involves an energized intermediate complex ($NiON_2$*):

$$\mathrm{Ni} + \mathrm{N_2O} \underset{k_{-1}}{\overset{k_1}{\rightleftarrows}} \mathrm{NiON_2^*} \xrightarrow{k_3[N_2]} \mathrm{NiON_2}$$
$$\mathrm{NiON_2^*} \xrightarrow{k_2} \mathrm{NiO} + \mathrm{N_2} \qquad (5)$$

then the experimentally observed rate constant is[28]

$$k_{obsd} = k_1\left(\frac{k_2 + k_3[N_2]}{k_{-1} + k_2 + k_3[N_2]}\right) \qquad (6)$$

According to this mechanism the Ni and N_2O react to form an energized complex, $NiON_2$*, with rate constant k_1. This complex can then be stabilized by collisions ($k_3[N_2]$) or can either react to produce NiO product (k_2) or decompose back to reactants (k_{-1}). Thus, the physical interpretation of eq 6 is that the experimentally observed rate constant is equal to the rate of energized complex formation multiplied by the fraction of energized complexes which do not decompose back to reactants. The only rate constant which can be determined absolutely from the data is k_1; only relative values of the other constants can be determined. Unfortunately, the parameters in eq 6 are not determined very well from our data; the error estimates are on the same order of magnitude as the ratios. Nevertheless, a nonlinear least-squares fit of the rate constants to eq 6 yields 1.7 × 10^{-12} molecule^{-1} cm^3 s^{-1} for k_1, and the ratios k_2/k_3 and k_{-1}/k_3 are 1.1 and 19 molecule cm^{-3}, respectively. These parameters yield essentially the same goodness of fit to the data as the parameters reported previously for the fit to eq 4. In the limit of zero buffer gas pressure, eq 4 reduces to

$$k_{obsd} = k_1\left(\frac{k_2}{k_{-1} + k_2}\right) = k_{abs} \qquad (7)$$

which corresponds to the rate of the abstraction reaction in the absence of the buffer. Substitution of the fitted parameters from eq 6 to eq 7 yield a value of 9.3 × 10^{-14} molecule^{-1} cm^3 s^{-1} for the rate constant of the abstraction channel in the absence of buffer gas. This value is the same as the value obtained from the fit to eq 4. The values determined for k_{abs} from the two fits are within the experimental uncertainty of the experimental value at 2.5 Torr; therefore, the abstraction channel appears to be the dominant channel at a pressure of 2.5 Torr.

An Arrhenius fit of the rate constants is complicated by the termolecular component of the reaction. It is expected that for increasing temperatures, the termolecular component contribution to the second-order rate constant will decrease while the abstraction channel component will increase. Consequently, the termolecular component should be negligible at all temperatures

TABLE 3: Ionization Potentials, sp Promotion Energies, Enthalpies of Reaction, and Experimental and Calculated Activation Barriers for the Reaction: TM(g) + N_2O(g) → TMO(g) + N_2(g)

metal	IP[a] (kJ/mol)	sp PE[a] (kJ/mol)	$\Delta H°$ [b] (kJ/mol)	E_a(model)[a] (kJ/mol)	E_a(experiment)[a] (kJ/mol)	ref
Sc($s^2d^1\ ^2D_{3/2}$)	631	187	−514	4.5	12.0	17
Ti($s^2d^2\ ^3F_2$)	658	193	−501	8.0	14.3	11
V($s^2d^3\ ^4F_{3/2}$)	651	196	−470	8.1	10.7	this work
Cr($s^1d^5\ ^7S_3$)	653	279	-291	20.8	21.1	this work
Mn($s^2d^5\ ^6S_{5/2}$)	717	220	−190	18.4	44.7	15
Fe($s^2d^6\ ^5D_4$)	762	231	−248	23.9	44.4	14
					49.4	30
Co($s^2d^7\ ^4F_{9/2}$)	759	282	−214	31.5	48.8	this work
Ni($s^2d^8\ ^3F_4$)	737	308	−215	32.7	11.3	this work
Cu($s^1d^{10}\ ^2S_{1/2}$)	745	365	−113	39.6	39.6	10
					48.6	31
Zn($s^2d^{10}\ ^1S_0$)	906	387	>−103	51.7	>65	this work
Y($s^2d^1\ ^2D_{3/2}$)	600	179	−542	2.2	4.0	32
Zr($s^2d^2\ ^3F_2$)	640	177	−628	2.6	3.3	26
Nb($s^1d^4\ ^6D_{1/2}$)	652	199	−595	8.9	∼0	22
Mo($s^1d^5\ ^7S_3$)	684	306	−431	28.1	41	33
Ru($s^1d^7\ ^5F_5$)	710	302	−346	29.9	38	34
Rh($s^1d^8\ ^4F_{9/2}$)	720	324	−254	33.2	1.3	25
La($s^2d^1\ ^2D_{3/2}$)	538	159	−634	0.0	∼0	32
Hf($s^2d^2\ ^3F_2$)	659	215	−651	8.1	11.3	26
Ta($s^2d^3\ ^4F_{3/2}$)	761	208	−672	17.5	13.6	23
W($s^2d^4\ ^5D_0$)	770	232	−508	22.6	25.6	24
Re($s^2d^5\ ^6S_{5/2}$)	760	227	−455	20.2	>50	35
Os($s^2d^6\ ^5D_4$)	843	281	−365	34.5	38.1	36
Ir($s^2d^7\ ^4F_{9/2}$)	873	315	−244	41.1	>45	37
Pt($s^1d^9\ ^3D_3$)	865	361	−225	46.2	∼6[c]	38

[a] Ref 20. [b] Refs 3 and 4. [c] Calculated from the rate constants reported in ref 38.

at a pressure of 2.5 Torr. Thus, assuming the rate constants at 2.5 Torr are solely due to the abstraction channel, the rate constants for the abstraction channel are fit in Arrhenius form by $k(T) = (5.9 \pm 2.0) \times 10^{-12}$ exp(11.4 ± 1.4 kJ/mol/R T) molecule^{-1} cm^3 s^{-1}. An Arrhenius plot of the rate constants is shown in Figure 6.

Honma and co-workers reported an upper bound for the room-temperature rate constant for this reaction of 5×10^{-14} molecule^{-1} cm^3 s^{-1} at a total pressure of 0.7 Torr using a fast-flow tube.[18] This upper bound is smaller than our extrapolated value of the bimolecular component. The fast flow method might give poor results in this instance due to cascading of excited states to the ground state along the length of the flow tube.

Zn($4s^2\ ^1S_0$). Temperature-dependent rate constant measurements were attempted up to a temperature of 623 K in N_2 buffer utilizing Zn(TMHD)$_2$ as precursor. Detection of zinc atoms was accomplished by both exciting and detecting the fluorescence from the $4p\ ^1P_1°-4s^2\ ^1S_0$ transition at 213.856 nm. A narrow-band interference filter centered at 214 nm was utilized to isolate the fluorescence. The rate of this reaction is extremely slow so that we can only report an upper limit. Detection of zinc atoms could be observed at 623 K in partial pressures of N_2O up to 89 Torr. The lifetime of zinc under these conditions was approximately 5000 μs. Based on these data, we report an upper limit for the reaction of Zn($4s^2\ ^1S_0$) at 623 K of 1×10^{-16} molecule^{-1} cm^3 s^{-1}. Assuming a preexponential factor of approximately the gas kinetic collision rate, we can place a lower limit on the activation energy of approximately 65 kJ/mol.

The only previously reported measurement of the rate constant for ground-state zinc reacting with N_2O is that by Raich and Belbruno utilizing a flow reactor.[6] The reported rate constant is $(1.8 \pm 0.5) \times 10^{-15}$ molecule^{-1} cm^3 s^{-1} at 303 K and a pressure of approximately 10 Torr. Fontijn has questioned the accuracy of this value because the magnitude of the rate constant appears to be higher than expected.[20] Their rate constant value is considerably higher than our upper limit despite our use of a temperature over 300 K higher than their room temperature measurement. Their value is most likely only an upper limit since their measured rate constant is near the lower limit of the useful range of the apparatus used.

Discussion

Table 3 lists the experimental activation energies for the transition metals measured thus far. The wide range of barrier heights indicates a complex relationship between the way the reactant potential energy surfaces evolve into products. To understand the reactions of transition metal atoms with N_2O, attention must be given to multidimensional intersections among diabatic potential energy surfaces arising from both ground and low-lying excited states of the reactants. The large number of low-lying states for many transition metals means numerous potential energy surfaces are accessible in the entrance channel. Many of the reactions of transition metals with N_2O have large exothermicities so that various product channels may be accessed. Consequently, the activation barrier is a complex interplay of how a transition metal's reactant surfaces evolve into the accessible product channels. Since all transition metal/N_2O reactions require transitions from reactant surfaces of O($^1D_2$) character to surfaces of O(^3P) character to access low-energy product states, barriers are expected unless other factors make alternative excited state channels (with possibly lower barriers) accessible. Transition metals with a large number of low-lying atomic states and a large number of low-lying excited states in its oxide are expected to increase the likelihood of a smaller barrier since alternate pathways with possible lower barriers than the ground-state reaction may become accessible. Furthermore, the greater the magnitude of the exothermicity, the more energy available to access metal oxide excited states. Thus, a reaction with a large exothermicity should improve the likelihood of a smaller barrier. Unfortunately, little is known about the potential energy surfaces for the interaction of transition metal atoms with nitrous oxide. A complete under-

standing of these reactions awaits advances in theoretical dynamics calculations for these systems.

Finally, we compare the experimentally determined barriers for these reactions with the values predicted from a semiempirical method developed by Fontijn and co-workers.[20] In this model, activation barriers are calculated by taking into account the ionization potential and sp promotion energy of the metal, the electron affinity of N_2O, and the bond energy of the metal oxide product. According to the model, the approach of the metal and nitrous oxide results in a large potential barrier due to both the weakening of the N−O bond and the repulsive exchange forces between the metal and N_2O. This barrier is substantially decreased by the addition of p character to one valence electron of the transition metal and by addition of ionic character to the transition metal and N_2O. The appearance of resonance energy in the activated complex is dictated mainly by the transition metal's promotion energy of an s electron to the lowest-energy p orbital and by the metal's ionization potential; therefore, these two properties largely determine the activation barrier.

In the resonance model, the activated complex is described by three resonance structures. The first structure has a covalent bond between the oxygen and the transition metal in which the transition metal uses the s orbital for bonding. The second structure also has a covalent bond except the transition metal has p character. The last structure results from the interaction of N_2O^- and TM^+. The activation energy is calculated on the basis of the wave functions of these structures and their contribution to the electronic structure. The resonance is described as the superposition of the distinct wave functions of each resonance structure. The calculations are based on the premise that the metal−oxygen bond is only of s and p character. The model does not account for the presence of d electrons on the transition metal or the electronic structure of the TM−O bond. According to the resonance theory, as the ionization potential and s−p promotion energy of the transition metal increase, the energy differences between the resonating structures should also increase. This causes the resonance energy to decrease and the activation energy to increase.

Along with the experimentally measured barriers, Table 3 presents a listing of the calculated activation barriers using Fontijn's resonance model. Obviously, a rudimentary model such as this resonance theory cannot be expected to accurately predict the barrier for every transition metal. As seen from Table 3, the model most successfully predicts the barriers for the first four metals of each transition metal series. For a majority of the remainder of the transition metals, the model tends to underestimate the barriers. The exceptions to this trend are nickel, rhodium, and platinum. Nickel and platinum exhibit complex dynamics which would not be expected to be modeled by the resonance theory. Rhodium exhibits near temperature-independent behavior, apparently due to its unusual electronic structure. The exact match with copper is due to the adjustable barrier parameter in the theory being based on this reaction. In conclusion, the semiempirical treatment for the calculation of activation energies yields moderately successful results and appears to be a useful method to estimate barriers for reactions which are difficult to determine experimentally.

Acknowledgment. This research was supported by a Cottrell College Science Award of Research Corporation. Acknowledgment is made to the donors of the Petroleum Research Fund, administered by the American Chemical Society, for partial support of this research. M.L.C. is a Henry Dreyfus Teacher-Scholar. I thank Professor Gary Fowler of the USNA Mathematics Department for performing the calculations to fit the nickel data to eq 6.

References and Notes

(1) Plane, J. M. C. In *Gas-Phase Metal Reactions*; Fontijn, A., Ed.; Elsevier: Amsterdam, 1992; p 29.
(2) Campbell, M. L. *J. Chem. Phys.* **1999**, *111*, 562.
(3) Chase, M. W., Jr.; Davies, C. A.; Downey, J. R., Jr.; Frurip, D. J.; McDonald R. A.; Syverud, A. N. *J. Phys. Chem. Ref. Data* **1985**, *14*, Suppl. 1.
(4) Wagman, D. D.; Evans, W. H.; Parker, V. B.; Schumm, R. H.; Halow, I.; Bailey, S. M.; Churney, K. L.; Nuttall, R. L. The NBS tables of chemical thermodynamic properties. *J. Phys. Chem. Ref. Data* **1982**, *11*, Suppl. 2.
(5) Jonah, C. D.; Zare, R. N.; Ottinger, C. J. *J. Chem. Phys.* **1972**, *56*, 263.
(6) Raiche, G. A.; Belbruno, J. J. *Chem. Phys. Lett.* **1987**, *134*, 341.
(7) Ritter, D.; Weisshaar, J. C. *J. Phys. Chem.* **1989**, *93*, 1576.
(8) Ritter, D.; Weisshaar, J. C. *J. Phys. Chem.* **1990**, *94*, 4907.
(9) Parnis, J. M.; Mitchell, S. A.; Hackett, P. A. *J. Phys. Chem.* **1990**, *94*, 8152.
(10) Narayan, A. S.; Futerko, P. M.; Fontijn, A. *J. Phys. Chem.* **1992**, *96*, 290.
(11) Campbell, M. L.; McClean, R. E. *J. Phys. Chem.* **1993**, *97*, 7942.
(12) Clemmer, D. E.; Honma, K.; Koyano, I. *J. Phys. Chem.* **1993**, *97*, 11480.
(13) Fontijn, A.; Blue, A. S.; Narayan, A. S.; Bajaj, P. N. *Combust. Sci. Technol.* **1994**, *101*, 59.
(14) Campbell, M. L.; Metzger, J. R. *Chem. Phys. Lett.* **1996**, *253*, 158.
(15) Campbell, M. L. *J. Chem. Phys.* **1996**, *104*, 7515.
(16) Plane, J. M. C.; Rollason, R. J. *J. Chem. Soc., Faraday Trans.* **1996**, *92*, 4371.
(17) Campbell, M. L.; Hooper, K. L.; Kölsch, E. J. *Chem. Phys. Lett.* **1997**, *274*, 7.
(18) Matsui, R.; Senba, K.; Honma, K. *J. Phys. Chem. A* **1997**, *101*, 179.
(19) Zaslonko, I. S.; Smirnov, V. N. *Kinet. Katal.* **1998**, *39*, 485.
(20) Futerko, P. M.; Fontijn, A. *J. Chem. Phys.* **1991**, *95*, 8065.
(21) Campbell, M. L.; McClean, R. E. *J. Chem. Soc., Faraday Trans.* **1995**, *91*, 3787.
(22) McClean, R. E.; Campbell, M. L.; Kölsch, E. J. *J. Phys. Chem. A* **1997**, *101*, 3348.
(23) Campbell, M. L.; Hooper, K. L. *J. Chem. Soc., Faraday Trans.* **1997**, *93*, 2139.
(24) Harter, J. S. S.; Campbell, M. L.; McClean, R. E. *Int. J. Chem. Kinet.* **1997**, *29*, 367.
(25) Campbell, M. L. *Laser Chem.* **1998**, *17*, 219.
(26) Campbell, M. L. *J. Chem. Soc., Faraday Trans.* **1998**, *94*, 353.
(27) Robinson, P. J.; Holbrook, K. A. *Unimolecular Reactions*; Wiley-Interscience: New York, 1972.
(28) Parnis, J. M.; Mitchell, S. A.; Hackett, P. A. *Chem. Phys. Lett.* **1988**, *151*, 485.
(29) Garland, N. L.; Douglass, C. H.; Nelson, H. H. *J. Phys. Chem.* **1992**, *96*, 8390.
(30) Plane, J. M. C.; Rollason, R. J. *J. Chem. Soc., Faraday Trans.* **1996**, *92*, 4371.
(31) Vinckier, C.; Verhaeghe, T.; Vanhees, I. *J. Chem. Soc., Faraday Trans.* **1994**, *90*, 2003.
(32) Campbell, M. L. *Chem. Phys. Lett.* **1998**, *294*, 339.
(33) McClean, R. E.; Campbell, M. L.; Goodwin, R. H. *J. Phys. Chem.* **1996**, *100*, 7502.
(34) Campbell, M. L. *J. Chem. Soc., Faraday Trans.* **1996**, *92*, 4377.
(35) Campbell, M. L. *J. Phys. Chem. A* **1998**, *102*, 892.
(36) Campbell, M. L. *J. Phys. Chem.* **1996**, *100*, 19430.
(37) Campbell, M. L. *J. Phys. Chem. A* **1997**, *101*, 9377.
(38) Campbell, M. L. *J. Chem. Soc., Faraday Trans.* **1998**, *94*, 353.